PHYSICAL REVIEW A **87**, 060303(R) (2013)

Exploring the effect of noise on the Berry phase

S. Berger,* M. Pechal, A. A. Abdumalikov, Jr., C. Eichler, L. Steffen, A. Fedorov,† A. Wallraff, and S. Filipp
Department of Physics, ETH Zurich, CH-8093 Zurich, Switzerland
(Received 13 February 2013; published 26 June 2013)

We experimentally investigate the effects of noise on the adiabatic and cyclic geometric phase, also termed the Berry phase. By introducing artificial fluctuations in the path of the control field, we measure the geometric contribution to dephasing of an effective two-level system for a variety of noise powers and different paths. Our results, measured using a microwave-driven superconducting qubit, clearly show that only fluctuations which distort the path lead to geometric dephasing. In a direct comparison with the dynamic phase, which is path independent, we observe that the Berry phase is less affected by noise-induced dephasing. This observation directly points towards the potential of geometric phases for quantum gates or metrological applications.

DOI: 10.1103/PhysRevA.87.060303 PACS number(s): 03.67.Lx, 03.65.Vf, 42.50.Pq, 85.25.Cp

Noise is ubiquitous in physical systems—be it thermal noise in electrical circuits [1], electronic shot noise in mesoscopic conductors [2], vacuum noise of radiation fields [3], or low-frequency ($1/f$-) noise in solid-state systems [4,5]. It prevents quantum coherence from persisting on long time scales and hinders the development of a large-scale quantum computer [6,7]. Significant effort has thus been put into concepts and methods to control and maintain fragile quantum superposition states [8]. The geometric phase is a promising building block for noise-resilient quantum operations [9] and its properties in open quantum systems have been actively investigated in theory [10–17]. There are, however, only a few experiments studying the contribution to dephasing stemming from the Berry phase [18–20].

In this Rapid Communication, we study the physics of a two-level system, a qubit, in an effective field $\mathbf{B}$, described by the Hamiltonian

$$H = \hbar\boldsymbol{\sigma}\cdot\mathbf{B}/2, \tag{1}$$

where $\boldsymbol{\sigma} = (X,Y,Z)$ are the Pauli matrices and $\mathbf{B} = (B_x, B_y, B_z)$ is given in units of angular frequency. If the field is adiabatically and cyclically varied in time, the ground $|0\rangle$ and excited state $|1\rangle$ of the two-level system acquire a geometric phase $\gamma_0 = \pm A/2$, where A is the solid angle (with respect to the origin $\mathbf{B} = \mathbf{0}$) enclosed by the path traced out by $\mathbf{B}(t)$ [21]. This type of geometric phase is known as Berry phase. Here, we consider an effective field evolving along a circular path with radius $B_\rho = \sqrt{B_x^2 + B_y^2}$ at constant B_z and with precession period τ (Fig. 1). This path encloses a solid angle $A = 2\pi(1 - \cos\vartheta)$, with the polar angle $\vartheta = \arctan(B_\rho/B_z)$.

In realistic situations, the field components fluctuate about their mean values and these fluctuations induce dephasing. Changes in field strength will cause dynamic dephasing, while modifications in solid angle will cause geometric dephasing. Clearly, noise directed in azimuthal direction [angular noise, Fig. 1(b)] does not modify the solid angle and thus, no geometric dephasing is expected. In contrast, noise directed in radial direction [radial noise, Fig. 1(c)] will lead to geometric contributions to dephasing. By artificially adding noise in the radial (or azimuthal) direction to the field in our experiment, we are thus able to maximize (or minimize) geometric dephasing and investigate its properties for different angles ϑ and noise powers.

To model realistic uncorrelated noise with a given bandwidth, we generate fluctuations conforming to Ornstein-Uhlenbeck processes, i.e., stationary, Gaussian, and Markovian noise processes with a Lorentzian spectrum of bandwidth Γ_i and noise power P_i $(i = \rho,\varphi)$. In the experiment, the precession frequency and the noise bandwidth are chosen to be small compared to the amplitude $B = |\mathbf{B}|$ of the effective field, i.e., $1/\tau, \Gamma_i \ll B$, to study adiabatic processes. In this case, we can derive the variance of the geometric phase from a perturbative treatment. To first order in the noise variations $\delta\varphi$ and $\delta\rho$, the deviation $\delta\gamma$ of the Berry phase is [11]

$$\delta\gamma = -\frac{\pi}{\tau}\int_0^\tau \sin\vartheta\,\delta\vartheta\,dt. \tag{2}$$

As the ensemble average of $\delta\gamma$ vanishes, the mean Berry phase is identical to γ_0. By expressing the effective field in cylindrical coordinates, $\mathbf{B} = (B_\rho\cos\varphi, B_\rho\sin\varphi, B_z)$, the variations in the polar angle can be written as $\delta\vartheta = (\cos\vartheta/B)\delta\rho$, and the Berry phase is found to have a Gaussian distribution with variance

$$\sigma_\gamma^2 = 2P_\rho\left(\frac{\pi\cos\vartheta\sin\vartheta}{B\tau}\right)^2\frac{\Gamma_\rho\tau - 1 + e^{-\Gamma_\rho\tau}}{\Gamma_\rho^2}. \tag{3}$$

As expected, to first order only variations $\delta\rho$ in radial direction contribute to σ_γ^2.

Geometric phases have been observed in a variety of superconducting systems [22–25]. Here, we use the two lowest energy levels of a superconducting artificial atom of the transmon type [26] embedded in a transmission line resonator—an architecture known as circuit quantum electrodynamics [27,28]. Note, however, that our findings are independent of the specific implementation, and apply to any system in which Berry phases can be observed. The qubit is manipulated using microwave fields applied via a capacitively coupled charge bias line. Using spectroscopic measurements, we have determined the maximum Josephson energy $E_{J,\max}/h = 11.4\,\text{GHz}$, the charging energy $E_C/h = 0.26\,\text{GHz}$, and the coupling strength $g/2\pi = 360\,\text{MHz}$ of the qubit to the resonator. The experiments are performed

*sberger@phys.ethz.ch
†Present address: School of Mathematics and Physics, University of Queensland, Brisbane QLD 4072, Australia.

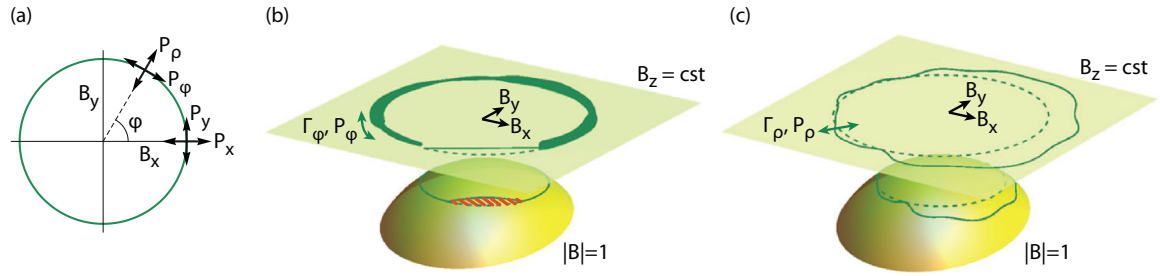

FIG. 1. (Color online) (a) The path of the effective field describes a circle in the B_x-B_y plane at constant B_z. Noise in x and y directions with noise powers P_x and P_y can be decomposed into noise in ρ and φ directions with noise powers P_ρ and P_φ. (b) and (c) The path of the effective field without noise (dashed lines lying in the plane with constant B_z) is drawn alongside the same path exposed to two kinds of noise (solid lines): angular noise in panel (b), where the velocity of precession is proportional to line thickness, and radial noise in panel (c). The projection of the paths on the unit sphere $|\mathbf{B}| = 1$ is also shown. In panel (b), the difference in solid angle due to noncyclic evolution is highlighted by a stripe pattern.

at a qubit transition frequency $\omega_{01}/2\pi = 4.68\,\mathrm{GHz}$, with an energy relaxation time $T_1 = 2.65\,\mu\mathrm{s}$, a phase coherence time $T_2 = 1.35\,\mu\mathrm{s}$, and a spin-echo phase coherence time $T_2^{\mathrm{echo}} = 2.15\,\mu\mathrm{s}$. The sample is operated in a dilution refrigerator at a base temperature of 20 mK. In the dispersive regime, when ω_{01} is far detuned from the resonator mode, the Hamiltonian of the driven system is [22]

$$H_{\mathrm{eff}} = \hbar(X\Omega\cos\varphi + Y\Omega\sin\varphi + Z\Delta)/2 \qquad (4)$$

in a reference frame which rotates at the drive frequency ω_d. This Hamiltonian is identical to the one in Eq. (1) with an effective field $\mathbf{B} = (\Omega\cos\varphi, \Omega\sin\varphi, \Delta)$. It is determined by amplitude Ω, phase angle φ and detuning $\Delta = \omega_{01} - \omega_d$ of the drive.

A Ramsey-type interferometric sequence containing a spin-echo pulse to cancel the dynamic phase [18,29] is employed to measure the Berry phase acquired by the two-level system [see Fig. 3(a)]. A series of resonant pulses (of frequency ω_{01}) implement the spin-echo sequence, while off-resonant pulses (of frequency $\omega_d = \omega_{01} - \Delta$) guide its state adiabatically along the paths sketched in Figs. 1(b) and 1(c).

All presented Berry phases are measured at a detuning $\Delta = -50\,\mathrm{MHz}$. The acquired Berry phase is varied from 0 to 6.9 rad by increasing the solid angle A via the drive amplitude Ω. The strength of the noise is quantified by the normalized noise amplitude $s_\rho = \sqrt{P_\rho}/B_\rho$ for radial noise and by $s_\varphi = \sqrt{P_\varphi}$ for angular noise. These definitions ensure that fluctuations in radial or azimuthal directions have identical amplitudes if $s_\rho = s_\varphi$.

The phases with noise are obtained by repeating the experiment with different noise patterns. Identical noise patterns are used before and after the spin echo pulse to ensure cancellation of the dynamical phase. The pulse sequences, consisting of two intermediate-frequency quadratures x and y, are numerically created: Noise conforming to an Ornstein-Uhlenbeck process is generated and added to the pulses describing the noiseless evolution of the field. An arbitrary waveform generator synthesizes these quadratures, which are up-converted to a microwave-frequency signal using an in-phase–quadrature (IQ) mixer. After the manipulation sequence, the state of the qubit is determined in a dispersive readout [30] through the resonator and reconstructed using state tomography [31]. To overcome noise in the detection, each individual noise realization is measured 10^6 times.

Histograms of the measured Berry phases for four solid angles are shown in Figs. 2(a)–2(d). For radial noise, the Berry phases of the individual noise realizations have—as discussed above—a Gaussian distribution with a mean equal to the Berry phase γ_0 without noise. For angular noise, we observe that the widths of the phase distributions are, as expected, almost zero. The expectation values of the Bloch-vector components $\langle X\rangle$ and $\langle Y\rangle$ for individual noise realizations are distributed on the equatorial plane of the Bloch sphere [Figs. 2(b) and 2(d)], reflecting the spread of the measured phases. They lie on a circle with radius $\nu_0 \approx 0.80 < 1$, which is a result of the intrinsic noise present in the system.

Distributions akin to those shown in Figs. 2(b) and 2(d) are used to compute the coherence $\nu = \sqrt{\langle X\rangle^2 + \langle Y\rangle^2} = e^{-(4\sigma_\gamma)^2/2}$ versus solid angle [Fig. 2(f)]. In this plot and all subsequent plots, the coherences are normalized to a measurement without added noise whereby the intrinsic noise is eliminated. We observe that for radial noise the coherence decreases and then stabilizes as a function of solid angle, while it is approximately unity for angular noise. This is an immediate consequence of the nature of the Berry phase: Radial noise modifies the solid angle A, causing dephasing and a decrease in coherence. In contrast, angular noise hardly affects A.

For both kinds of noise, the difference $\Delta\gamma = \gamma - \gamma_0 \lesssim 0.2$ rad in the mean Berry phase with and without noise is very small [Fig. 2(e)]. The measured coherences agree well with Eq. (3) and numerical results obtained by solving the unitary dynamics of the Hamiltonian in Eq. (4). The measured Berry phase γ_0 itself (not shown) agrees well with the prediction for a transmon-type qubit [25], with a discrepancy of 0.20 rad across all solid angles for the data in Figs. 2(e) and 2(f).

To illustrate the effects of noise quantitatively, both the Berry phase and the dynamic phase are measured for varying noise amplitudes s. For the Berry phase, we observe that the coherence follows the expected dependence $e^{-(4as)^2/2}$ for radial noise [Figs. 3(c) and 3(e)] and that angular noise has a lesser effect on the coherence than radial noise. For both types of noise, and for normalized noise amplitudes $\lesssim 0.5$, the Berry phase with and without noise have the same value.

The coherence of the dynamic phase δ can be computed perturbatively, in the same way as for the Berry phase. Using the deviation $\int_0^\tau \delta B\,dt/\hbar = \int_0^\tau \sin\vartheta\,\delta\rho\,dt/\hbar$ of the dynamic

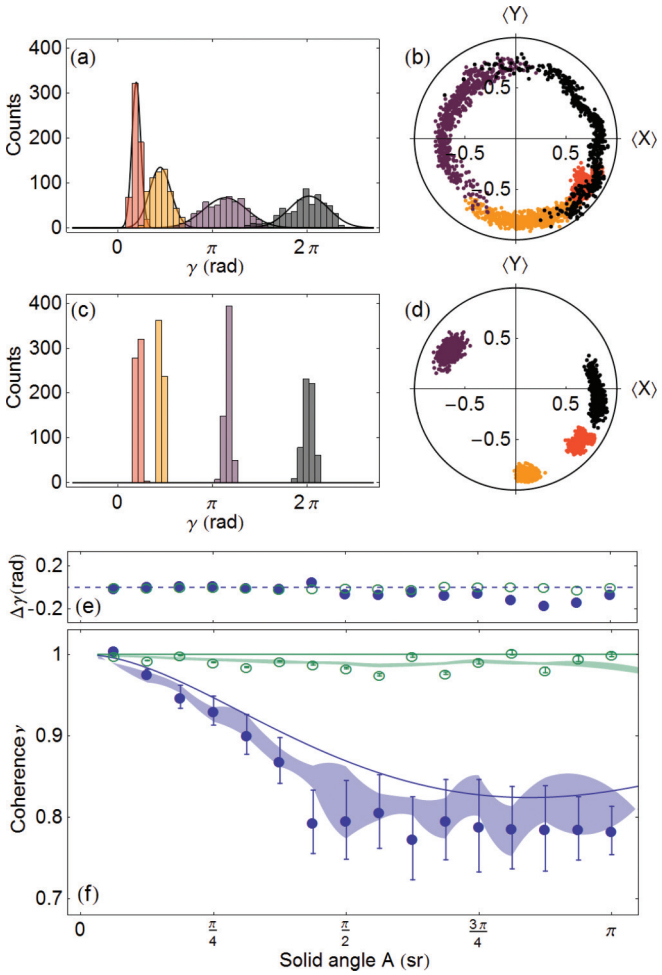

FIG. 2. (Color online) (a) Histograms of Berry phases and (b) measured expectation values $\langle X\rangle$, $\langle Y\rangle$ of 600 realizations of radial noise for each solid angle $A = \pi/16, 3\pi/16, 8\pi/16$, and $15\pi/16$ (indicated in red, orange, purple, and black online). Fits of a Gaussian to the measured histograms are also shown in panel (a). The circle in panel (b) indicates unit coherence. (c) and (d) Measurements analogous to panels (a) and (b) for angular noise. (e) and (f) Coherence ν and phase difference $\Delta\gamma$ as a function of solid angle A for radial noise (filled circles) and angular noise (open circles). The experimental data points are shown alongside the theory curve (solid lines) and the results from numerical simulations (the shaded area indicates the standard deviation about the mean). Data in panels (a)–(f) are recorded at fixed noise bandwidths $\Gamma_i = 10$ MHz, normalized noise amplitudes $s_i = 1/15$, and evolution time $\tau = 100$ ns.

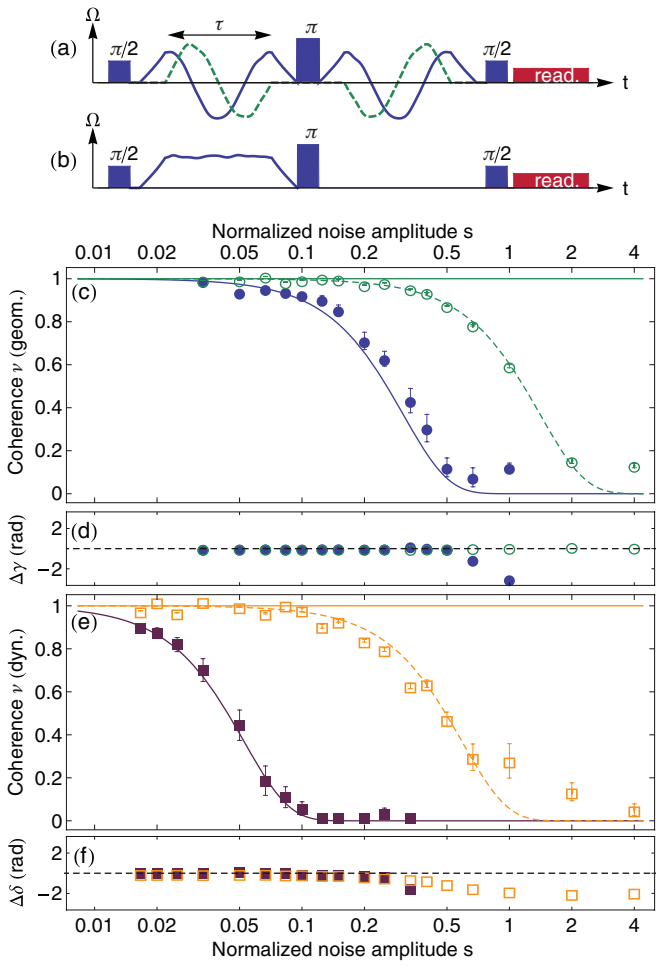

FIG. 3. (Color online) (a) and (b) Sketches of the pulse schemes used to measure (a) Berry and (b) dynamic phases with radial noise. Pulses applied along the x and y quadratures are shown as solid and dashed lines, respectively. The readout pulse (see text) concludes the sequence after $t \approx 400$ ns. (c) and (d) Experimentally measured coherence ν of the Berry phase and phase difference $\Delta\gamma = \gamma - \gamma_0$ as a function of normalized noise amplitude s for radial noise (filled circles) and angular noise (open circles), plotted on a logarithmic scale. For every value of s, 300 noise realizations were measured with noise bandwidth $\Gamma = 10$ MHz at solid angle $A = 7\pi/16$ and evolution time $\tau = 100$ ns. The continuous line is computed from Eq. (3). The dashed line is a fit to the function $\exp(-(4as)^2/2)$ with fitting parameter $a = 0.25 \pm 0.01$. (e) and (f) Quantities analogous to panels (c) and (d) but for the dynamic phase, with $\Delta\delta = \delta - \delta_0$ and fitting parameter $a = 0.60 \pm 0.03$.

phase, one finds its mean δ and its variance

$$\sigma_\delta^2 = 2P_\rho(\sin\vartheta)^2\frac{\Gamma_\rho\tau - 1 + e^{-\Gamma_\rho\tau}}{\Gamma_\rho^2}. \quad (5)$$

Only radial variations contribute to σ_δ^2 and cause the dynamic phase to have a Gaussian distribution around the noiseless dynamic phase δ_0. Noise in azimuthal direction does not change the magnitude of the field and hence does not cause fluctuations in the dynamic phase.

The coherence of the dynamic phase was recorded using a spin-echo sequence containing a single off-resonant pulse [Fig. 3(b)], and therefore its variance was scaled by a factor to allow for direct comparison with the Berry phase. From Fig. 3(e), it is evident that the coherence of the dynamic phase starts decreasing at weaker noise amplitudes than the Berry phase, demonstrating the superior noise resilience of the Berry phase. It is also observed that the mean dynamic phase δ starts deviating from δ_0 already at $s \approx 0.2$. The measured coherences for both dynamic and Berry phase are in very good agreement with the predictions based on Eqs. (3) and (5) for radial noise. For angular noise, fits to $e^{-(4as)^2/2}$ agree with the observed behavior of the coherences. Indeed, while according to Eqs. (3) and (5) the coherences are expected to be insensitive to angular

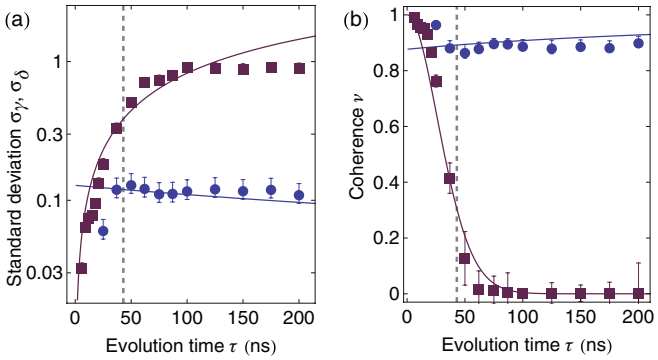

FIG. 4. (Color online) (a) Standard deviation σ_γ of the Berry phase (dots) and σ_δ of the dynamic phase (squares) as a function of evolution time τ, based on 300 noise realizations with $\Gamma = 10\,\mathrm{MHz}$ and $s_\rho = 1/15$. The solid lines result from calculations based on Eqs. (3) and (5). The vertical dashed line approximately separates the nonadiabatic from the adiabatic regime. (b) Coherence ν vs evolution time τ of the Berry phase (dots) and the dynamic phase (squares).

noise to first order, nonadiabatic and higher-order effects [32] still affect the coherences. In particular, the evolution of the field can be noncyclic [33], which adds a small contribution to dephasing [11] [Fig. 1(b)].

Finally, we directly compare the coherence of dynamic and Berry phases in the presence of radial noise. The Berry phase γ is recorded at a solid angle $A = 0.37\pi$, where the effect of noise on γ is strongest. For long evolution times τ, the Berry phase is more resilient against radial noise than the dynamic phase because its variance σ_γ^2 decreases with evolution time [18], whereas the variance of the dynamic phase σ_δ^2 grows linearly in evolution time [cf. Eqs. (3) and (5), as well as Fig. 4]. Both phases have equal coherences when $\sigma_\gamma^2 = \sigma_\delta^2$, i.e.,

$$\tau = \pi \cos(\vartheta)/B, \tag{6}$$

and the dynamic phase is more coherent than the Berry phase only for even shorter evolution times [$\tau < 13$ ns according to Eq. (6) and $\tau < 20$ ns according to the experimental data in Fig. 4]. Note that the variance of the dynamic phase is independent of the value of the dynamic phase, which is why it was recorded using the same drive amplitudes as for the Berry phase gates. The data in Fig. 4 agree with calculations. The standard deviation σ_δ of the dynamic phase starts differing significantly from computed predictions at evolution times $\tau \gtrsim 100\,\mathrm{ns}$, when the recorded phases are spread across 2π and their variance saturates.

In conclusion, we have demonstrated that the Berry phase is less affected by noise along the path in parameter space than by noise perpendicular to it. Given a system with known noise properties, this can potentially be exploited to realize noise-resilient geometric operations. Both kinds of noise leave the mean of the geometric phase unchanged. Shifts of the mean Berry phase are theoretically expected [12] but are beyond current experimental precision. We have also shown that the geometric phase is less affected by decoherence than the dynamic phase when evolving adiabatically (evolution times $\gtrsim 1/B$). Our results beautifully exemplify fundamental properties of the geometric phase and serve as a stepping stone for further investigations of geometric phases as a resource for quantum computation or for precision measurements [34–37].

S.B. thanks A. Agazzi for help with numerical simulations. This work was supported by the Swiss National Science Foundation (SNF) and the EU project GEOMDISS.

[1] F. N. H. Robinson, *Noise and Fluctuations in Electronic Devices and Circuits* (Clarendon Press, Oxford, 1974).
[2] Y. M. Blanter and M. Büttiker, Phys. Rep. **336**, 1 (2000).
[3] R. J. Glauber, Phys. Rev. **130**, 2529 (1963).
[4] P. Dutta and P. M. Horn, Rev. Mod. Phys. **53**, 497 (1981).
[5] J. Bylander, S. Gustavsson, F. Yan, F. Yoshihara, K. Harrabi, G. Fitch, D. G. Cory, Y. Nakamura, J.-S. Tsai, and W. D. Oliver, Nat. Phys. **7**, 565 (2011).
[6] M. Schlosshauer, *Decoherence and the Quantum-to-Classical Transition* (Springer, Heidelberg, 2007).
[7] E. Joos, H. D. Zeh, C. Kiefer, D. J. W. Giulini, J. Kupsch, and I.-O. Stamatescu, *Decoherence and the Appearance of a Classical World in Quantum Theory* (Springer, Heidelberg, 2003).
[8] T. D. Ladd, F. Jelezko, R. Laflamme, Y. Nakamura, C. Monroe, and J. L. O'Brien, Nature (London) **464**, 45 (2010).
[9] E. Sjoqvist, Physics **1**, 35 (2008).
[10] A. Blais and A. M. S. Tremblay, Phys. Rev. A **67**, 012308 (2003).
[11] G. De Chiara and G. M. Palma, Phys. Rev. Lett. **91**, 090404 (2003).
[12] R. S. Whitney, Y. Makhlin, A. Shnirman, and Y. Gefen, Phys. Rev. Lett. **94**, 070407 (2005).
[13] R. S. Whitney and Y. Gefen, Phys. Rev. Lett. **90**, 190402 (2003).
[14] A. Carollo, I. Fuentes-Guridi, M. F. Santos, and V. Vedral, Phys. Rev. Lett. **90**, 160402 (2003).
[15] P. Solinas, M. Möttönen, J. Salmilehto, and J. P. Pekola, Phys. Rev. B **82**, 134517 (2010).
[16] P. I. Villar and F. C. Lombardo, Phys. Rev. A **83**, 052121 (2011).
[17] P. Solinas, M. Sassetti, P. Truini, and N. Zanghì, New J. Phys. **14**, 093006 (2012).
[18] S. Filipp, J. Klepp, Y. Hasegawa, C. Plonka-Spehr, U. Schmidt, P. Geltenbort, and H. Rauch, Phys. Rev. Lett. **102**, 030404 (2009).
[19] F. M. Cucchietti, J.-F. Zhang, F. C. Lombardo, P. I. Villar, and R. Laflamme, Phys. Rev. Lett. **105**, 240406 (2010).
[20] H. Wu, E. M. Gauger, R. E. George, M. Möttönen, H. Riemann, N. V. Abrosimov, P. Becker, H.-J. Pohl, K. M. Itoh, M. L. W. Thewalt, and J. J. L. Morton, Phys. Rev. A **87**, 032326 (2013).
[21] M. V. Berry, Proc. R. Soc. London, Ser. A **392**, 45 (1984).
[22] P. J. Leek, J. M. Fink, A. Blais, R. Bianchetti, M. Göppl, J. M. Gambetta, D. I. Schuster, L. Frunzio, R. J. Schoelkopf, and A. Wallraff, Science **318**, 1889 (2007).
[23] M. Möttönen, J. J. Vartiainen, and J. P. Pekola, Phys. Rev. Lett. **100**, 177201 (2008).

[24] M. Neeley, M. Ansmann, R. C. Bialczak, M. Hofheinz, E. Lucero, A. D. O'Connell, D. Sank, H. Wang, J. Wenner, A. N. Cleland, M. R. Geller, and J. M. Martinis, Science **325**, 722 (2009).

[25] S. Berger, M. Pechal, S. Pugnetti, A. A. Abdumalikov, Jr., L. Steffen, A. Fedorov, A. Wallraff, and S. Filipp, Phys. Rev. B **85**, 220502(R) (2012).

[26] J. Koch, T. M. Yu, J. Gambetta, A. A. Houck, D. I. Schuster, J. Majer, A. Blais, M. H. Devoret, S. M. Girvin, and R. J. Schoelkopf, Phys. Rev. A **76**, 042319 (2007).

[27] A. Blais, R.-S. Huang, A. Wallraff, S. M. Girvin, and R. J. Schoelkopf, Phys. Rev. A **69**, 062320 (2004).

[28] A. Wallraff, D. I. Schuster, A. Blais, L. Frunzio, R.-S. Huang, J. Majer, S. Kumar, S. M. Girvin, and R. J. Schoelkopf, Nature (London) **431**, 162 (2004).

[29] J. A. Jones, V. Vedral, A. Ekert, and G. Castagnoli, Nature (London) **403**, 869 (2000).

[30] R. Bianchetti, S. Filipp, M. Baur, J. M. Fink, M. Göppl, P. J. Leek, L. Steffen, A. Blais, and A. Wallraff, Phys. Rev. A **80**, 043840 (2009).

[31] M. G. A. Paris and J. Řeháček (eds.), *Quantum State Estimation*, Lecture Notes in Physics, Vol. 649 (Springer, Berlin, 2004).

[32] C. Lupo and P. Aniello, Phys. Scr. **79**, 065012 (2009).

[33] J. Samuel and R. Bhandari, Phys. Rev. Lett. **60**, 2339 (1988).

[34] E. Martín-Martínez, A. Dragan, R. B. Mann, and I. Fuentes, New J. Phys. **15**, 053036 (2013).

[35] X. Rong, P. Huang, X. Kong, X. Xu, F. Shi, Y. Wang, and J. Du, Europhys. Lett. **95**, 6 (2011).

[36] I. Pikovski, M. R. Vanner, M. Aspelmeyer, M. S. Kim, and C. Brukner, Nat. Phys. **8**, 393 (2012).

[37] J. Mur-Petit, J. J. García-Ripoll, J. Pérez-Ríos, J. Campos-Martínez, M. I. Hernández, and S. Willitsch, Phys. Rev. A **85**, 022308 (2012).